International Journal of Radiation Oncology biology • physics

www.redjournal.org

Biology Contribution

Pharmacologic Inhibition of HIF-1α Attenuates Radiation-Induced Pulmonary Fibrosis in a Preclinical Image Guided Radiation Therapy

Jae-Kyung Nam, MS,*,† A-Ram Kim, PhD,* Seo-Hyun Choi, PhD,* Ji-Hee Kim, MS,*,† Su Chul Han, PhD,‡ Seungwoo Park, PhD,‡ Yong Jin Lee, PhD,§ Joon Kim, PhD,† Jaeho Cho, MD, PhD,‖ Hae-June Lee, DVM, PhD,* and Yoon-Jin Lee, PhD*

**Division of Radiation Biomedical Research, Korea Institute of Radiologic and Medical Sciences, Seoul, Korea; †Laboratory of Biochemistry, Division of Life Sciences, Korea University, Seoul, Korea; ‡Comprehensive Radiation Irradiation Center, Korea Institute of Radiologic and Medical Sciences, Seoul, Korea; §Division of Applied RI, Korea Institute of Radiologic and Medical Sciences, Seoul, Korea; and ‖Department of Radiation Oncology, Yonsei University College of Medicine, Seoul, Korea*

Received May 11, 2020. Accepted for publication Sep 6, 2020.

Purpose: Radiation-induced pulmonary fibrosis (RIPF) is a long-term side effect of thoracic radiation therapy. Hypoxia-induced vascular endothelial mesenchymal transition (EndMT) can occur during the development of RIPF. Here, we examined the direct contribution of endothelial HIF-1α (EC-HIF1α) on RIPF.

Methods and Materials: An inducible Cre-lox-mediated endothelial *Hif1a* deletion mouse line was used to evaluate the potential of HIF-1α inhibition to suppress RIPF. To evaluate the effects of a pharmacologic HIF-1α inhibitor on RIPF after image guided radiation therapy (IGRT) for spontaneous lung adenocarcinoma, we generated conditional tdTomato; K-Ras^{G12D}; and p53 $^{flox/flox}$ mice to facilitate tracking of tumor cells expressing tdTomato.

Results: We found that vascular endothelial-specific HIF-1α deletion shortly before radiation therapy inhibited the progression of RIPF along with reduced EndMT, whereas prolonged deletion of endothelial HIF-1α before irradiation did not. Moreover, we revealed that postirradiation treatment with the novel HIF-1α inhibitor, 2-methoxyestradiol (2-ME) could efficiently inhibit RIPF and EndMT. In addition, IGRT using primary mouse models of non-small cell lung cancer showed that combined treatment of 2-ME with ablative high-dose radiation therapy efficiently inhibited RIPF and the growth of both multifocal and single tumors, concomitantly reducing radiation-induced EndMT of normal as well as tumor regions.

Corresponding author: Yoon-Jin Lee, PhD; E-mail: yjlee8@kirams.re.kr

All data associated with this study are present in the paper or the Supplementary Materials.

S.-H. Choi's current affiliation is Department of Surgery, Memorial Sloan Kettering Cancer Center, New York City, New York.

This work was supported by grants from the National Research Foundation (NRF-2017M2A2A7A02019482/2020M2D9A2093964 and NRF-2020R1A2B5B02002709), and a grant from the Korea Institute of Radiologic and Medical Sciences (KIRAMS, 50531-2020) funded by the Ministry of Science and ICT (MSIT), Republic of Korea.

Disclosures: The authors declare no potential conflicts of interest.

Supplementary material for this article can be found at https://doi.org/10.1016/j.ijrobp.2020.09.006.

Int J Radiation Oncol Biol Phys, Vol. 109, No. 2, pp. 553–566, 2021

https://doi.org/10.1016/j.ijrobp.2020.09.006

Conclusion: These results suggest that a negative regulator of HIF-1α–mediated EndMT, such as 2-ME, may serve as a promising inhibitor of RIPF in radiation therapy.

Introduction

More than 70% of patients with thoracic cancer receive radiation therapy (RT).[1-3] During radiation therapy, radiation-induced lung injury (RILI), such as pneumonitis and fibrosis, can cause morbidity such as scarring of lung tissue and breathing difficulties, and is therefore considered as a treatment-limiting factor. In particular, 13% to 37% of patients with lung cancer, who receive RT, are susceptible to the development of radiation pneumonitis or fibrosis in the early or late phase of treatment, respectively.[4,5] Although recent improvements to radiation treatment modalities, such as stereotactic body radiation therapy (SBRT), have minimized the extent of targeted tissue and therefore the risks to nontargeted tissue, radiation-induced pneumonitis and fibrosis remain the most common toxicities associated with SBRT of lung cancer.[6,7] However, despite numerous studies, little progress has been made to reduce RILI; the medications developed for its reduction including steroids, ACE inhibitors, and pentoxifylline[8] have shown limited efficacy.

As an alternative, relevant animal models have been used to study radiation-induced lung fibrosis (RIPF) in cancer therapy and its amelioration using medications. In vivo RIPF studies have been performed mainly in the thoracic-irradiated normal lung.[9,10] An experimental RIPF model using focal ablative RT with high-dose irradiation can simulate clinical stereotactic radiation therapy (SBRT).[11,12] Specifically, delivering a single dose of 75 or 90 Gy irradiation to the left lung of mice caused inflammation and prefibrotic or fibrotic damage at 2 weeks postirradiation.[12,13] Moreover, to evaluate the efficacy of RT for cancer, human tumor features have been considered using genetically engineered mouse models (GEMM).[14] Unlike transplanted tumor models, RIPF studies using GEMMs may recapitulate the immune system and other normal tissues in the microenvironment around tumors. Therefore, a preclinical RIPF animal model of image guided RT (IGRT) for a GEMM-based single lung tumor or multifocal tumors may be useful as a preclinical platform.

The endothelial cell-to-mesenchymal transition (EndMT) can predominantly be observed in radiation-induced normal tissue damage.[12,15,16] EndMT is a phenomenon characterized by the loss of cell–cell junctions and acquisition of invasive and mesenchymal phenotypes, for example, in the process of cardiac and liver fibrosis.[17,18] Mesenchymal markers (eg, alpha-SMA, FSP-1, and vimentin) are upregulated, whereas endothelial cell (EC)–specific adhesion markers (eg, CD31 and VE-cadherin) are downregulated in the EndMT process. Hypoxia-induced vascular EndMT occurs during RIPF and is dependent on the hypoxia inducible factor 1 alpha (HIF-1α) expression of vascular ECs in human irradiated lung tissues.[12] The tumor vascular EndMT predominantly appears in tumor regrowth after radiation therapy for non-small cell lung cancer (NSCLC), and modulation of EndMT inhibits tumor regrowth, ultimately affecting tumor immunity and cancer stem cell proliferation.[19] Thus, negatively regulating vascular EndMT may enhance the efficacy of radiation therapy, thereby inhibiting tumor regrowth and RIPF. One anticancer drug, 2-methoxyestradiol (2-ME), approved by the US Food and Drug Administration (FDA) and successfully used in clinical treatment for breast, prostate, and ovarian cancer,[20,21] can function as an HIF-1α inhibitor[22,23]; it also inhibits radiation-induced EndMT by reducing HIF1 expression in human umbilical vein endothelial cells (HUVECs) and limits RIPF after 16 Gy thoracic irradiation in vivo.[12]

In the present study, we examined the direct contribution of endothelial HIF-1α (EC-HIF1α) in RIPF using a GEMM to affect tamoxifen-inducible CreERT2-mediated EC-*Hif1a* deletion in addition to the effect of 2-ME administration. Deleting EC-Hif1α shortly before focal irradiation significantly inhibited vascular EndMT and subsequent RIPF development, whereas these benefits were not observed at prolonged deletion before radiation therapy. Consistently, 2-ME treatment after but not considerably before ablative high-dose radiation therapy inhibited RIPF and reduced EndMT. Furthermore, evaluation of the effects of 2-ME on RIPF after IGRT for spontaneous lung adenocarcinoma in conditional $Kras^{G12D};Trp53^{flox/flox}$ mice revealed an increase in tumor radiosensitivity. Together, these findings suggest that targeting EC-HIF1α with 2-ME might constitute a therapeutic strategy to increase the efficacy of radiation therapy by negatively regulating radiation-induced EndMT.

Methods and Materials

Study design

The goals of this study were to demonstrate the role of vascular endothelial HIF-1α as a regulator of radiation-induced EndMT, on RIPF and to suggest a promising inhibitor of RIPF. We used genetically engineered mice to define the role of endothelial HIF-1α and observed histology and immunofluorescence images. Temporal HIF-1α deletion was performed using a tamoxifen-inducible gene deletion system. Thoracic radiation dose and volume were selected based on a previous study. Fibrosis was quantified

by the Ashcroft score of hematoxylin and eosin (H&E) staining and the collagen deposition in Masson trichrome staining. EndMT was quantified by $SMA^{+}CD31^{+}$ endothelial area of immunofluorescence. To perform IGRT for spontaneous tumors, we estimated tumor formation using IVIS every week. When a single tumor size was 100 to 150 mm^3, IGRT was performed. All animal experiments were approved by the Institutional Animal Care and Use Committee of the Korea Institute of Radiologic & Medical Sciences and are reported in accordance with the Animal Research: Reporting of In Vivo Experiments (ARRIVE) guidelines.[24] All studies were performed in triplicate. Histologic quantification was performed in a double-blind manner.

Mice

Specific pathogen-free *Cdh5*-CreERT2 mice were purchased from Taconic Biosciences (Rensselaer, NY), whereas specific pathogen-free C57BL/6 *Tie2*-Cre, $HIF1a^{flox/flox}$, $Trp53^{flox/flox}$, LSL-$Kras^{G12D}$, and CAG-tdTomato mice were purchased from Jackson Laboratory (Bar Harbor, ME). *Cdh5*-CreERT2;$HIF1a^{+/+}$, *Cdh5*-CreERT2$^{-/-}$, or *Tie2*-Cre$^{-/-}$ littermates were used as controls. C57BL/6 mice were purchased from Orient Bio Inc (Seongnam, South Korea). All animal experimental data shown are representative of 3 independent experiments. All experiments were conducted with 7- to 8-week-old mice. Mice had ad libitum access to standard diet and water. All mice were anesthetized with a combination of anesthetics before being sacrificed.

Radiation-induced fibrosis model

Radiation was delivered using the X-RAD 320 platform (Precision X-ray, North Branford, CT) as previously described.[25] The left main bronchi of 7- to 8-week-old mice were irradiated at 90 Gy using a 3-mm diameter field to mimic an ablative dose. *Cdh5*-CreERT2;$Hif1\alpha^{fl/fl}$ mice were injected intraperitoneally with 1 mg of tamoxifen (Sigma, St Louis, MO; dissolved in corn oil) once daily for 5 days starting 2 or 11 days before irradiation. C57BL/6 mice were treated with 2-ME (30, 60 mg/kg, intraperitoneally; 60 mg/kg, by mouth), amifostine (30 mg/kg, intraperitoneally), or pirfenidone (30 mg/kg, intraperitoneally) 1 hour before irradiation, and dosing continued every 2 to 3 days for a total of 6 doses. In the posttreatment group, C57BL/6 mice were treated with 2-ME (60 mg/kg, intraperitoneally) 4 days after irradiation, and dosing continued every 2 days for a total of 5 doses. Further, 2-ME (Selleckchem, Houston, TX), amifostine (Selleckchem), and pirfenidone (Selleckchem) (30 mg/kg, intraperitoneally) were dissolved in 2% (v/v) dimethylsulfoxide (DMSO) + 30% (w/v) polyethylene glycol (PEG) 300 + 1% (v/v) Tween 80 + ddH_2O, water, and 2% (v/v) DMSO + 30% (w/v) PEG 300 + ddH_2O, respectively, immediately before injection.

Primary tumor model

LSL-Kras^{G12D};*Trp53*$^{fl/fl}$ mice have been described previously.[14] Single nodule and multinodule lung adenocarcinomas were respectively induced via intrathoracic and intranasal administration of a prepackaged Ad-Cre adenovirus (Cell Biolabs, San Diego, CA). After 7 weeks, mouse thoracic regions were irradiated with 16 Gy (X-RAD 320 platform). The angiogenesis inhibitor, 2-ME, was dissolved in DMSO and further diluted in 30% (w/v) PEG-400 solution with 1% (v/v) Tween 80 immediately before intraperitoneal injection. The administration of 2-ME began 1 hour before irradiation, and dosing continued once daily for 10 days at 150 mg/kg (first 4 days) and 30 mg/kg (subsequent 6 days). Each experimental group contained 6 mice. FDG-PET scans were performed 0, 5, 10, and 20 days after irradiation, as previously described[26] (Siemens Medical Solutions, Munich, Germany). Mouse lung tissues were obtained 1 and 2 months after irradiation. To evaluate tumor progression, tumor nodules were counted in H&E-stained lung tissue sections. For the local tumor model, *LSL-Kras*^{G12D};*Trp53*$^{fl/fl}$;CAG-tdTomato mice were injected with a Cre adenovirus by inserting a needle through the fourth left intercostal space of the posterior chest wall. After 7 weeks, the tumoral area of the left lung in mice was irradiated at a dose of 75 Gy using a 5-mm diameter field. Administration of 2-ME began 1 hour before irradiation and dosing continued every 2 to 3 days for a total of 6 doses. Micro-CT scans were performed 0, 2, and 4 weeks after irradiation using a commercial small-animal micro-CT scanner under general anesthesia with 2% isoflurane. CT images were analyzed using ASIProVM software (Concorde Microsystems, Knoxville, TN). tdTomato immunofluorescence images were captured using an IVIS-200 system (Xenogen, Alameda, CA) under isoflurane anesthesia. Mouse lung tissues were obtained at 4 weeks after irradiation.

Small animal irradiation planning and IGRT

An image guided precision irradiator (XRAD-SmART, Precision X-ray) was used to deliver a single high dose (75 Gy) to the left lung tumor in mice. This system consisted of an x-ray irradiation system, precision collimators for small fields, and an image guide system using a cone beam CT and moving stage. A single dose of 75 Gy was delivered to the target using an opposed tangential field (Gantry angle 350° and 170°) and a 5-mm collimator to protect the opposite lung and spinal cord. SmART-plan version 1.5.0 was used for precise targeted irradiation planning. The

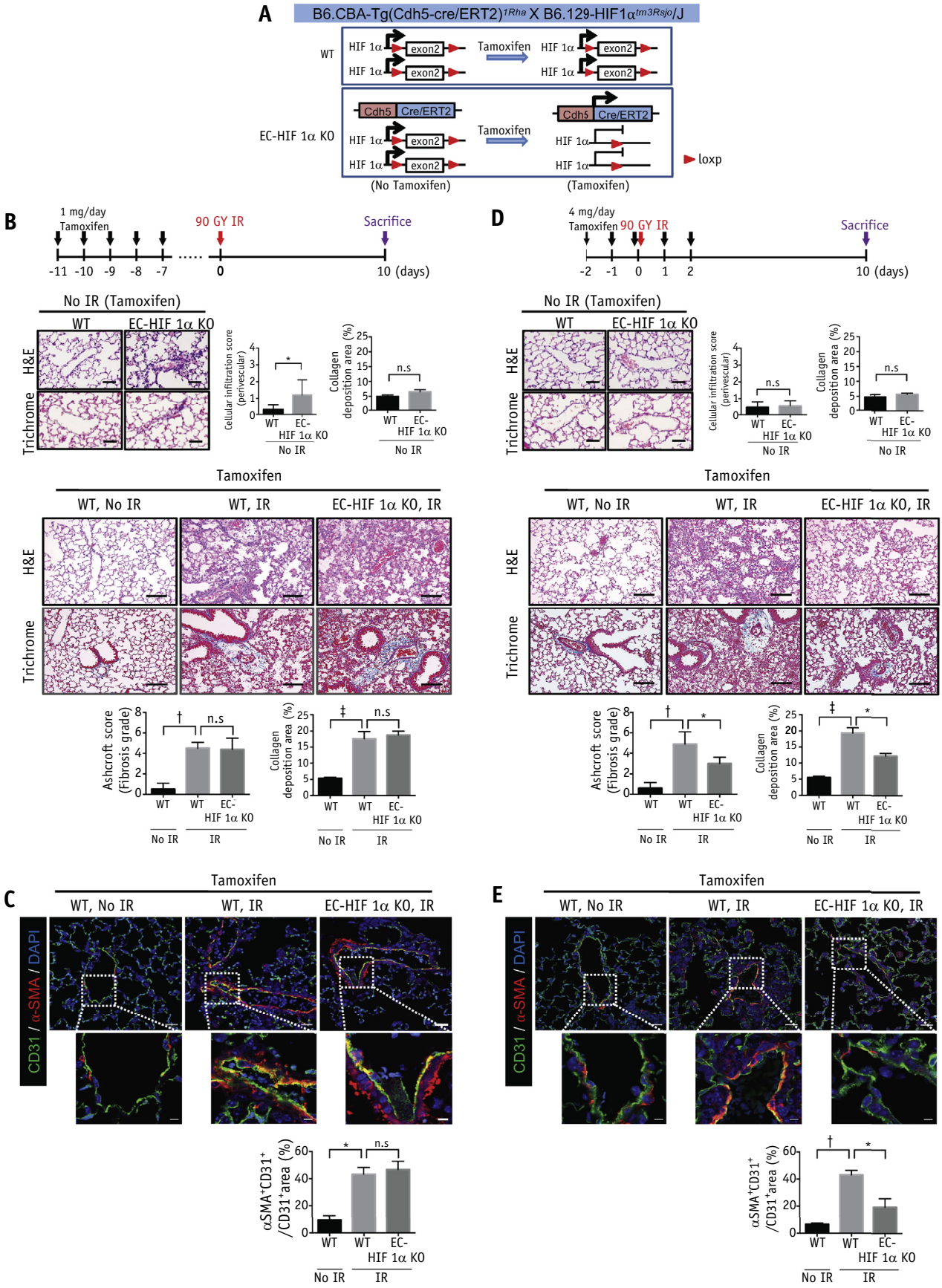

Fig. 1. Endothelial specific HIF-1α deletion inhibits radiation-induced lung fibrosis and EndMT. *Hif1a*$^{flox/flox}$ (WT) and *Cdh5*-CreERT2;*Hif1a*$^{flox/flox}$ (EC-HIF1αKO) mice (A) were treated with tamoxifen daily for 5 days starting at 11 (B, C) or 2

irradiation settings were 225 kV, 13 mA, large focal size, and Cu filter with a dose rate of 3.45 Gy/min. The procedure for dose calculation was performed as described in the AAPM Task Group 61 Report.[27]

Microcone beam CT (micro-CBCT)

The micro-CBCT used in this study included the parameters 40 kV, 3 mA, small focal size, and an Al filter that could be used by changing the tube voltage and x-ray tube setting. The system used an amorphous silicon flat-panel detector with pixel size of 200 μm (Perkin-Elmer, Wiesbaden, Germany).

Histology and immunofluorescence staining

Tissues were covered with optimal cutting temperature (OCT) compound (Sakura Finetek; VWR, IL) and snap-frozen on dry ice or fixed in 10% (v/v) neutral-buffered formalin, embedded in paraffin, and sectioned. The sections were deparaffinized and stained as previously described.[12] The staining procedure for the OCT sections was the same as that for the paraffin-embedded sections, except that antigen removal was omitted. Immunofluorescence staining was carried out using primary antibodies against CD31 (1:200; #AF3628; R&D Systems, Minneapolis, MN), αSMA (1:1000; #A5228; Sigma-Aldrich), Hif-1α (1:100; #sc-53546; Santacruz), Hif-2α (1:200; #PA1-16510; Invitrogen), and NG2 (1:500; #AB5320; Millipore, Billerica, MA). Fibrosis grade was determined based on the Ashcroft score.[28] Collagen deposition was assessed using Masson trichrome staining (Polyscience). We measured collagen deposition at the same position of irradiated lung tissues (in the pulmonary vessel and bronchi area) for accuracy of quantification. In case of a severe fibrotic region with no vascular structures owing to damaged vessels, we quantified the collagen composition around alveolar tissues while avoiding the vessel and bronchi regional area for an exact comparison. At least 5 images per section were acquired for quantification, and the positively stained areas were evaluated using Image J software. At least 5 images per section were acquired for quantification, and positively stained areas were evaluated using ImageJ software (NIH, Bethesda, MD; http://imagej.net/).

Cell culture and tube formation assay

HUVECs and human pericytes were obtained from PromoCell (Sungwoo Life Science, Uijeongbu, South Korea) and cultured in Endothelial Cell Growth Medium 2 and Pericyte Growth Medium, respectively (PromoCell) under 5% CO_2. HUVECs and pericytes were used within 9 passages. Cells were irradiated with gamma rays from a ^{137}Cs source (Atomic Energy of Canada, Chalk River, Canada) at 3.81 Gy/min. To assess the integration of pericytes into capillaries, HUVECs were irradiated and seeded onto Matrigel (BD Bioscience, San Jose, CA) in the presence or absence of pericytes, and analyzed at 4 hours after seeding. Before seeding, HUVECs and pericytes were fluorescently labeled with Q tracker 565 and Vybrant Multicolor Cell-Labeling DiO and DiI (1:500, Molecular Probes, Eugene, OR), respectively, according to the manufacturer's instructions.

Statistical analyses

Student *t* test and 1-way analysis of variance for multiple comparisons (for all others) were used to compare the experimental groups in GraphPad Prism version 5.0 (La Jolla, CA). A P value $< .05$ was considered significant. Experimenters were blinded to the group assignments and outcome assessments.

Results

EC-specific HIF-1α deletion temporal dependently affects RIPF by regulating EndMT

To determine whether deletion of EC-HIF1α could directly regulate RIPF development, EC-HIF1α KO mice were established by systemic tamoxifen-mediated specific Cre recombination driven by the vascular endothelial-cadherin promoter (Fig. 1A). To evaluate the effect of ablative high-dose radiation similar to SBRT, a single dose of 90 Gy administered with a 3-mm collimator was delivered to the left lung of mice. When tamoxifen was administered for 11 days before irradiation, EC-HIF1α deletion did not affect the progress of RIPF as evaluated by the Ashcroft score and collagen deposition, or of radiation-induced EndMT (Fig. 1B and 1C).

days (D, E) before irradiation to induce recombination, respectively. Lung tissues were obtained from nonirradiated mice and after focal 90 Gy irradiation (day 10) (n = 5-7 animals per group). (B, D) Hematoxylin & eosin staining and Masson trichrome staining in lung tissues, and scoring of fibrosis grade and quantification of collagen deposition per field (magnification, 200×). Scale bar = 100 μm. (C, E) Immunofluorescence staining of CD31 and αSMA in lung tissues at 10 days postirradiation (scale bar = 20 μm, scale bar of cropped images = 5 μm). Quantification of the $\alpha SMA^{+}CD31^{+}/CD31^{+}$ area as an average of 5 fields (magnification, 100×). For the Ashcroft score in graphs B and D, error bars indicate SD. For other graphs, error bars indicate SEM. $^{*}P < .01$, $^{\dagger}P < .001$, and $^{\ddagger}P < .0001$, ns: not significant (1-way ANOVA for multiple comparison). Data are representative of 3 independent experiments. *Abbreviations:* IR = irradiation; KO = knockout; WT = wild-type.

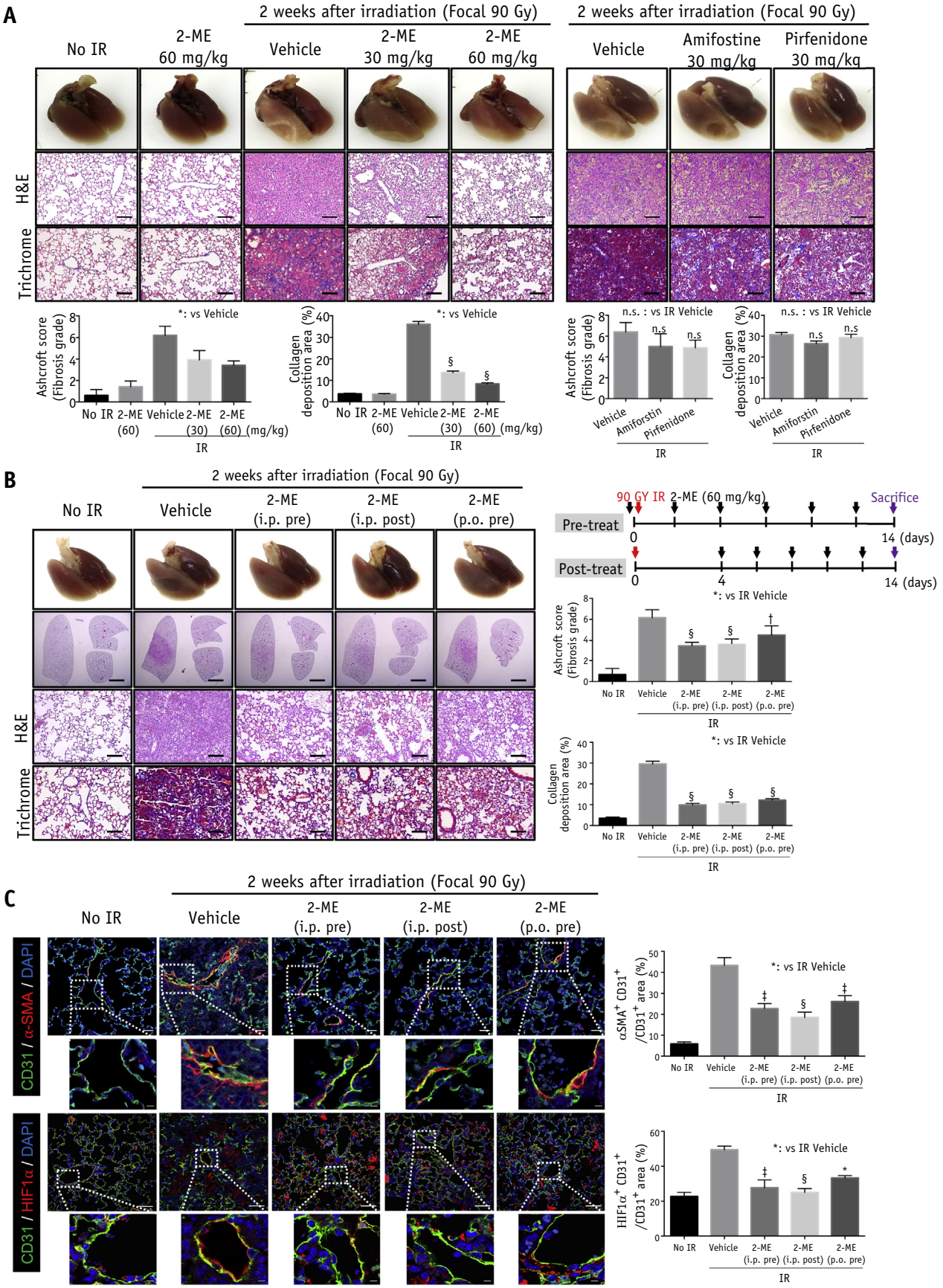

Fig. 2. 2-ME inhibits radiation-induced lung fibrosis and EndMT. (A) Representative images of the lungs, hematoxylin & eosin staining, and Masson trichrome staining in lung tissues from C57BL/6 mice 2 weeks after irradiation (IR), with or

However, 11 days after tamoxifen treatment, vascular damage with cell infiltration increased without irradiation, whereas collagen deposition did not[29] (Fig. 1B, upper images). Therefore, we adjusted the schedule of tamoxifen treatment and observed that tamoxifen treatment 2 days before irradiation did not induce vascular damage such as cell infiltration and collagen deposition (Fig. 1D, upper images). The change in morphologic patterns of damaged vessels was easily detected at 10 days after radiation rather than at 14 days in the fibrotic phase with severe vascular damage (Fig. 1). At 10 days after radiation, the fibrosis process began and resulted in collagen deposition to the parenchymal tissues. Therefore, we examined the early stage of radiation-induced vascular damage with the fibrotic phase in EC-HIF1α-deleted mice at 10 days after radiation. Moreover, EC-HIF1α deletion 2 days before irradiation inhibited the development of RIPF as estimated by the Ashcroft score and collagen deposition, also reducing radiation-induced vascular EndMT (Fig. 1D and 1E). As tamoxifen is known to have a direct effect on processes such as angiogenesis,[30] we compared the phenotype of WT mice with and without tamoxifen treatment in nonirradiated conditions to assess the direct effects of tamoxifen (Fig. E1A and E1B). The nonirradiated WT phenotype was not changed by tamoxifen treatment (Fig. 1B and 1D and Fig. E1A and E1B). Furthermore, in EC-HIF1α KO mice without tamoxifen treatment, EC-HIF1α could not be deleted in nonirradiated lungs, and they did not show vascular damage such as cellular infiltration (Fig. E1A). Figure E1, parts C and D, shows that HIF-1α was successfully knocked out in the EC of irradiated lung tissues

The HIF-1α inhibitor, 2-ME, inhibits RIPF in ablative high-dose RT

To evaluate whether upregulated EC-Hif1α after RT may constitute a valid target for inhibiting radiation-induced vascular damage and RIPF, we next evaluated the effects of 2-ME on RIPF in ablative high-dose RT. Compared with normal tissues, morphologic changes in irradiated lung tissues were observed in the irradiated area at 2 weeks after 90 Gy focal irradiation with a 3-mm collimator (Fig. 2A). As shown by H&E and trichrome staining, irradiation significantly induced fibrotic changes and collagen deposition. However, intraperitoneal injection of 2-ME efficiently inhibited RIPF in a dose-dependent manner, as evidenced by the Ashcroft score and collagen deposition (Fig. 2A, left). Furthermore, the radio-protective and antifibrotic effects of 2-ME were higher than those of amifostine, a synthetic sulfhydryl compound approved by the FDA as a radio-protector, and of pirfenidone, which was recently developed as a pharmacologic treatment for idiopathic pulmonary fibrosis[31,32] (Fig. 2A, right).

To further validate the pharmacology of 2-ME, we compared its effects on RIPF when administered intraperitoneally on alternative days starting 1 hour before or 4 days after irradiation (Fig. 2B). Posttreatment with 2-ME also appeared to significantly inhibit the RIPF occurring at 2 weeks after irradiation, as evidenced by the Ashcroft score and collagen deposition (Fig. 2B) in the irradiated lung tissue. These results suggest that 2-ME exerts both preventive and therapeutic efficacy on RIPF (Fig. 2B). Oral administration of 2-ME also reduced RIPF significantly (Fig. 2B). Notably, 2-ME treatment concomitantly inhibited radiation-induced EndMT at 2 weeks after focal exposure to high-dose radiation (90 Gy) (Fig. 2C).

HIF-1α and HIF-2α bind to the hypoxia response elements (HRE)[33]; endothelial HIF-2 α is well known to regulate hypoxic pulmonary hypertension.[34] We examined the effects of 2-ME on endothelial HIF-1α and HIF-2α expression in RIPF development (Fig. E2B and E2C). Two weeks after irradiation, both HIF-1α and HIF-2α expression was significantly upregulated in irradiated lung tissues compared with that in nonirradiated tissues. Radiation-induced HIF-1α expression was increased by 3-fold compared with HIF-2α expression (Fig. E2B). 2-ME effectively inhibited

without inhibitors (2-ME, amifostine, or pirfenidone). Scoring of fibrosis grade and quantification of collagen deposition per field (magnification, 200×) is shown. Scale bar = 100 μm. Mice were intraperitoneally (i.p.) injected with 2-ME, amifostine, pirfenidone, or vehicle, 1 hour before irradiation, and dosing continued every 2 to 3 days for a total of 6 times. Lung tissues were obtained from nonirradiated animals and after focal 90 Gy irradiation (day 14) (n = 6 animals per group). (B, C) C57BL/6 mice were i.p. or orally (p.o.) administered 2-ME starting 1 hour before or 4 days after irradiation as described in Materials and Methods. C57BL/6 mice were administered 2-ME i.p. (pretreatment) or p.o. (pretreatment) starting 1 hour before irradiation, and dosing continued every 2 to 3 days for a total of 6 doses. For the post-treatment group, C57BL/6 mice were injected i.p. (post-treatment) with 2-ME starting 4 days after irradiation, and dosing continued every 2 days for a total of 5 doses. Lung tissues were obtained from nonirradiated mice and after a focal 90 Gy irradiation (day 14) (n = 5-7 animals per group). (B) Representative images of lungs, hematoxylin & eosin staining, and Masson trichrome staining in lung tissues, schematic of 2-ME treatment strategies, and scoring of fibrosis grade and quantification of collagen deposition per field (magnification, 200×). Scale bar = 100 μm. (C) Immunofluorescence staining of CD31 and αSMA in lung tissues (scale bar = 20 μm, scale bar of cropped images = 5 μm). Immunofluorescence staining of CD31 and HIF-1α in lung tissues (scale bar = 50 μm, scale bar of cropped images = 5 μm). Quantification of the $\alpha SMA^{+}CD31^{+}/CD31^{+}$ area and the $HIF\text{-}1\alpha^{+}CD31^{+}/CD31^{+}$ as an average of 5 fields (magnification, 100×). For the Ashcroft score in graphs A and B, error bars indicate SD. For other graphs, error bars indicate SEM. $*P < .05$, $^{\dagger}P < .01$, $^{\ddagger}P < .001$, and $^{\S}P < .0001$, ns: not significant (1-way ANOVA for multiple comparison). Data are representative of 3 independent experiments.

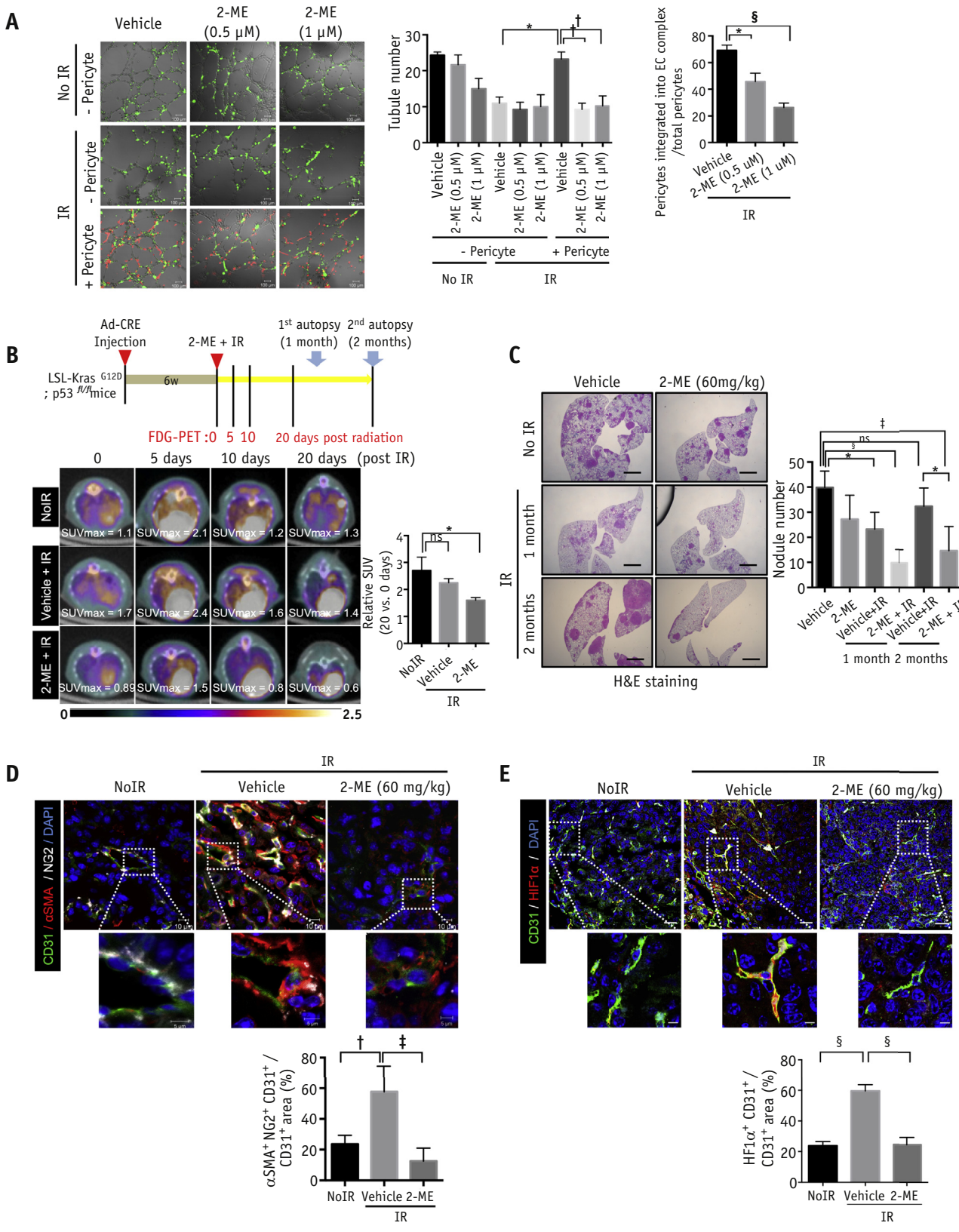

Fig. 3. 2-ME inhibits pericytes integration into endothelial cell (EC) and increases radio-response of spontaneous lung tumors, showing reduced tumor EndMT. (A) Effect of 2-ME on HUVEC tube formation in the presence and absence of pericytes after irradiation (IR). Tube numbers per field and fraction of pericytes integrated into EC complexes (200× magnification) are given. Error bars indicate the mean ± SD, n = 4. (B) FDG-PET/CT imaging of non-small cell lung cancers (NSCLCs) in LSL-*Kras*^{G12D};*Trp53*$^{flox/flox}$ (LSL-Kras^{G12D};p53 $^{fl/fl}$) mice that received 16 Gy thoracic radiation, with or without 2-ME. At 6

endothelial HIF-1α expression, but slightly reduced HIF-2α expression (Fig. E2B). Immunoblotting assay also showed that irradiation at a dose of 10 Gy increased HIF-1α and HIF-2 expression on ECs by 7.32-fold and 1.70-fold, respectively, and that 2-ME significantly inhibited HIF-1α and HIF-2α expression (Fig. E2C). From these results, we cautiously suggest that 2-ME affects RIPF by inhibiting radiation-induced HIF-1α expression to a greater extent than radiation-induced HIF-2α.

To verify whether 2-ME might be suitable as a therapeutic agent against RIPF in high-dose radiation therapy and SBRT, a single toxicity study was also performed with different doses (60, 150, and 300 mg/kg) of 2-ME intraperitoneally administered to mice. Notably, no effect on body weight was observed (Fig. E2). As shown in Table E1, the liver, spleen, and lung did not significantly differ after 2 weeks of 2-ME administration at 300 mg/kg. After a single administration, 2-ME did not produce any toxicity.

2-ME inhibits tumor EndMT and enhances spontaneous lung tumor radio-response

It was previously reported that targeting tumor EndMT inhibits tumor vasculature, including abnormal pericyte recruitment in tumor regrowth after RT.[19] This was revealed using isolated tumor cells from a spontaneous NSCLC (NSCL-KP tumor) model in which inhalation of a replication-deficient adenovirus expressing Cre (Ad-Cre) initiated activation of oncogenic K-Ras^{G12D} and deletion of both copies of a conditional p53 ($p53^{flox}$) allele by the Cre-*loxP* system.[14] Based on these reports, we hypothesized that a pharmacologic approach targeting radiation-induced tumor EndMT would inhibit tumor vasculature expansion and consequently inhibit tumor growth and metastasis after RT. First, in an in vitro assay, we showed that 2-ME inhibited pericyte integration into irradiated EC complexes in addition to tubule formation (Fig. 3A), which had been suggested to regulate tumor vasculature with pericyte recruitment.[19] Therefore, we next determined whether 2-ME might also inhibit tumor endothelial HIF-1α expression and subsequently tumor EndMT during tumor regrowth after RT. To evaluate the effect of 2-ME on tumor radiation response, the tumor response to 16 Gy irradiation in the thoracic area was assessed using fluorodeoxyglucose-positron emission tomography (FDG-PET). Tumor metabolism at 20 days after irradiation (6 weeks after Ad-Cre infection) was suppressed compared with that of control tumors. Irradiation combined with 2-ME was markedly more effective than either treatment alone for suppressing tumor metabolism (Fig. 3B). Furthermore, H&E staining confirmed that the treatment combination dramatically delayed tumor growth compared with that with irradiation alone (Fig. 3C). These results demonstrated that 2-ME increased the radio-response of NSCLCs.

As expected, irradiation triggered tumor EndMT with a concomitant increase in SMA$^+$ NG2$^+$ vessels, whereas these were inhibited when irradiation was combined with 2-ME (Fig. 3D). In addition, the upregulated HIF-1α$^+$ vessels that accompanied tumor EndMT were efficiently reduced after treatment with 2-ME (Fig. 3E).

2-ME inhibits RIPF in IGRT for single- and multifocal tumors

As lung tissues bearing tumors are considered to be complex tissues, including aberrant infiltrating immune cells, vascular cells, and extracellular matrix,[35] we hypothesized that the tumor microenvironment can affect RIPF occurrence in antitumor RT. Therefore, as a more clinically relevant model of RT, we further examined the effect of 2-ME on RIPF in IGRT for spontaneous murine lung tumors. To this end, we generated tdTomato; K-Ras^{G12D}; p53KO mice to facilitate the tracking of tumor cells expressing tdTomato initiated by the application of Adeno-Cre (Fig. 4A). First, a single-nodule tumor was generated by intrathoracic application of Adeno-Cre, and then tdTomato$^+$ tumors were detected using an in vivo imaging system (IVIS) (Fig. 4A). Tumor nodules ranged from 100 to 150 mm^3 within 3 to 4 weeks.

Furthermore, a beam of 75 Gy was applied to the left lung tumor using a 5-mm collimator to protect the opposite lung and spinal cord, as shown in Figure 4B. Computed tomography (CT) images of the lung were then used to predict fibrosis or pneumonitis. At 2 or 4 weeks after 75 Gy focal irradiation, the typical micro-CT manifestations in RILI were observed including ground-glass opacities and pulmonary consolidation (Fig. 4C).[36] These phenomena were significantly reduced by oral administration of 2-ME concomitant with significant tumor growth arrest compared with that in nonirradiated lungs (Fig. 4C). In

weeks following Ad-Cre administration, FDG-PET/CT images were obtained and the mice were irradiated. FDG-PET/CT imaging was repeated 5, 10, and 20 days following irradiation. (C) Representative images of hematoxylin & eosin staining of autologous lung adenocarcinoma from LSL-Kras^{G12D};p53 $^{fl/fl}$ mice after Ad-Cre injection and irradiation (left), and average nodule number per mouse (right) (10× magnification) were quantified (scale bar = 20 μm). Error bars indicate the mean ± SEM (no IR, n = 6; IR, n = 7; IR + 2-ME, n = 6). Data are representative of 2 independent experiments. (D, E) Immunofluorescence detection of CD31, αSMA, and NG2 (D), and CD31 and HIFα (E) in NSCLCs from LSL-Kras^{G12D};p53 $^{fl/fl}$ mice 2 months after irradiation, with or without 2-ME. αSMA$^+$NG2$^+$CD31$^+$ per CD31$^+$ area and HIFα$^+$ CD31$^+$ area per CD31$^+$ area (200× magnification) were quantified (scale bar = 20 μm, scale bar of cropped images = 5 μm). Error bars indicate the mean ± SEM, n = 6. $^*P < .05$, $^\dagger P < .01$, $^\ddagger P < .001$, and $^\S P < .0001$, ns: not significant 1-way ANOVA for multiple comparison). *Abbreviation:* SUV = standard FDG uptake value of the tumor.

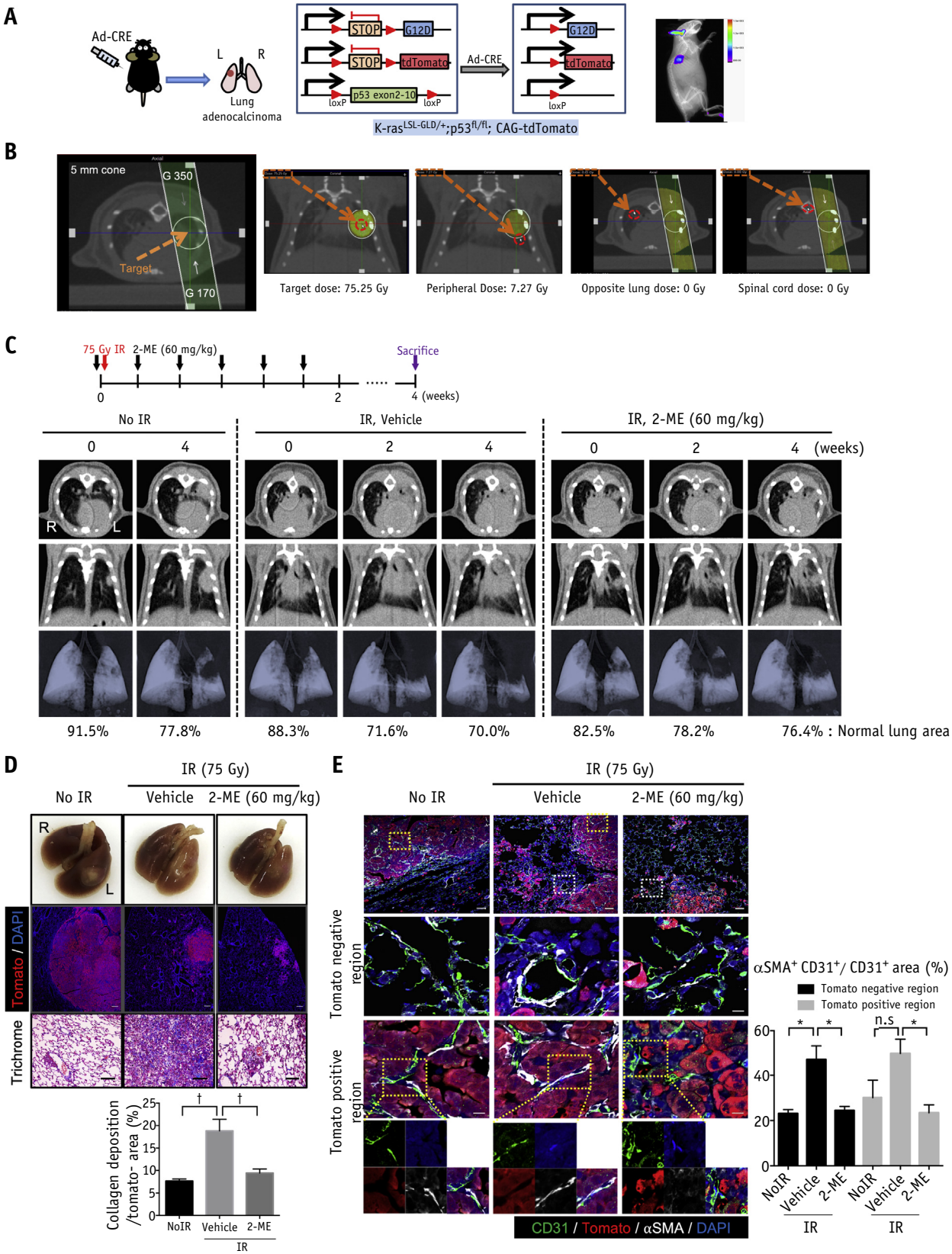

Fig. 4. 2-ME inhibits radiation-induced pulmonary fibrosis (RIPF) and delays tumor growth in image guided radiation therapy for single-nodule non-small cell lung cancer. (A) Schematic diagram of the local lung adenocarcinoma model and in vivo fluorescence imaging of tdTomato-labeled primary tumors. Left lung of *LSL-Kras^{G12D};Trp53$^{fl/fl}$*;CAG-tdTomato mice were locally intrathoracically injected with Ad-CRE virus to induce single-nodule primary lung adenocarcinoma. (B) Precise

addition, normal lung volume after IGRT was greater after combined treatment with 2-ME than that with vehicle (Fig. 4C).

Trichrome staining showed that 2-ME reduced collagen deposition on irradiated normal cells (Fig. 4D); moreover, the population of tomato-positive tumor cells could be distinguished from normal lung cells (Fig. 4D and 4E). At 4 weeks after RT, EndMT in tomato-normal areas and tomato$^+$ tumoral areas that appeared in the irradiated area were efficiently inhibited by treatment with 2-ME (Fig. 4E).

To elucidate the effects of 2-ME on RIPF after RT of multifocal tumors, multi-NSCLC tumor nodules were generated by intranasal Adeno-Cre application (Fig. 5A), which involved a beam of 75 Gy being applied to the left lung multitumor nodules using a 5-mm collimator to encompass the left multitumor volume (Fig. 5B). As a result, 2-ME markedly reduced RIPF compared with the effects of vehicle, thereby causing a reduction in ground-glass opacities and pulmonary consolidation and increased normal lung volume after IGRT (Fig. 5B). Trichrome staining showed that 2-ME reduced collagen deposition on irradiated normal cells and the population of tomato-positive tumor cells (Fig. 5C). EndMT and HIF-1α$^+$ vessels in both the tomato-normal area and the tomato$^+$ tumoral area were also reduced by treatment with 2-ME (Fig. 5D).

Discussion

Here, using an inducible Cre-lox-mediated *Hif1a* deletion mouse line, we found that vascular endothelial-specific HIF-1α deletion shortly, albeit not extensively, before RT inhibited the progression of RIPF along with reduced EndMT, as did post-RT administration of the HIF-1α inhibitor 2-ME, suggesting targeting post-RT-elevated HIF-1α as a new mechanism to reduce RIPF. Moreover, IGRT using primary mouse models of NSCLC showed that combined treatment of 2-ME with ablative high-dose RT efficiently inhibited RIPF along with radiation-induced EndMT while simultaneously increasing radiosensitivity of both single and multifocal tumors. Collectively, these results suggested that a negative regulator of HIF-1α-mediated EndMT, such as 2-ME, may serve as a promising inhibitor of RIPF in radiation therapy.

The role of hypoxia in radiation-induced normal tissue damage has been previously reported.[12] In response to hypoxia, it is well established that HIF-1α and HIF-2α regulate angiogenesis via vascular endothelial growth factor.[37] However, the hypoxia-dependent mechanism of HIF function in radiation-induced normal tissue damage remains unclear. In this study, we found that both HIF-1α and HIF-2α expression were upregulated in RIPF development and inhibited by 2-ME treatment. However, the inhibitory effect of 2-ME on HIF-1α was higher than that on HIF-2α expression in RIPF. In further study, the role of HIF-2α in RIPF and the effects of 2-ME on RIPF via inducible HIF-2α-deleted mice will be investigated.

Tie-2-promotor−specific Hif-1α deletion did not display protective effects against acute radiation syndrome after abdominal irradiation.[38] Recently, Toullec et al. revealed that in the acute exposure of the intestine to localized radiation after exteriorization, endothelial HIF-1α-deletion protects against radiation-induced enteritis, whereas epithelial HIF-1α-deletion does not.[39] Moreover, the reported effects of vascular HIF-1 on normal tissue injury are contradictory.[40-42] In a study conducted by Bryant et al., vascular endothelial HIF-1α was revealed to protect against pulmonary hypertension consequent to chronic hypoxia.[41] Recently, Lavigne et al. also reported that in HIF-1α floxed/VECad-Cre$^{+/-}$ mice, endothelial HIF-1α deletion reduced acute lung edema and neutrophil infiltration after lung stereotactic RT, but not long-term damage such as impaired running performance.[43] EndMT during RIPF development was mainly detected in HIF-1α−positive vascular ECs of hypoxic regions.[12] By using HIF-1α floxed/VECad-Cre-ERT2$^{+/-}$ mice, in the present study we demonstrated that prolonged deletion of endothelial HIF-1α before irradiation did not protect against RIPF development, whereas short-term deletion before RT exhibited an inhibitory effect by regulating radiation-induced EndMT. These conflicting results might therefore occur due to the status of vascular damage consequent to HIF-1α deletion at specific times before RT. Prolonged deletion of endothelial HIF-1α increased vascular damage such as cellular infiltration without irradiation, which in turn can accelerate radiation-induced normal tissue damage.

targeted irradiation planning SmART-plan system and dose of the main region. Target dose in coronal view, peripheral region dose of the target in coronal view, opposite lung dose and spinal cord dose with 75 Gy using a 5-mm cone. Each dose indicates the point dose of the irradiation planning system. (C) Micro-CT images of the entire thorax in *LSL-Kras^{G12D};Trp53$^{fl/fl}$*;CAG-tdTomato mice that received 75 Gy focal irradiation (IR), with or without 2-ME. At 4 weeks after Ad-Cre administration, horizontal (upper), transaxial (middle), and 3D micro-CT (bottom) images were acquired from nonirradiated animals (0, 4 weeks) and after a focal 75 Gy irradiation (0, 2, 4 weeks). Quantification of normal lung area is shown. (D) Representative images of lungs, immunofluorescence staining of tdTomato (scale bar = 200 μm) and Masson trichrome staining (scale bar = 100 μm). (E) Immunofluorescence staining of αSMA, tdTomato, and CD31 (scale bar = 50 μm, scale bar of cropped images = 10 μm) in lung tissues from (C). Quantification of collagen deposition per field (left panel; magnification, 200×) and the αSMA$^+$CD31$^+$/CD31$^+$ area as an average of 5 fields (right panel; magnification, 100×). For all graphs, error bars indicate SEM. $^*P < .05$, $^\dagger P < .01$, ns: not significant (1-way ANOVA for multiple comparison). Data are representative of 3 independent experiments.

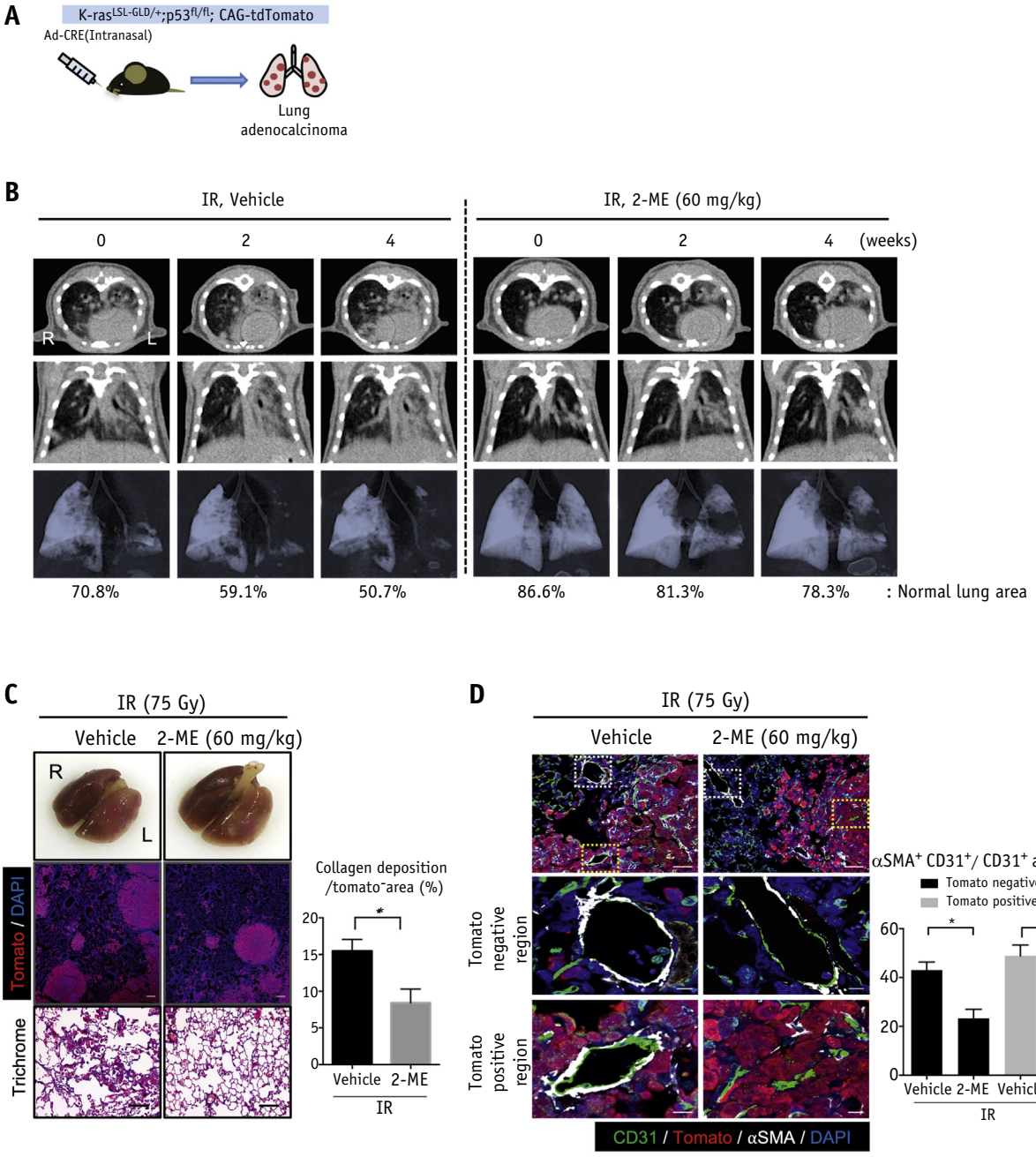

Fig. 5. 2-ME inhibits radiation-induced pulmonary fibrosis and tumor growth of multinodule non-small cell lung cancer after irradiation. (A) *LSL-Kras^{G12D};Trp53$^{fl/fl}$;*CAG-tdTomato mice were intranasally infected with Ad-CRE virus to induce multinodule primary lung adenocarcinoma. Left lung multitumors were irradiated with 75 Gy using a 5-mm cone. (B) Micro-CT images of the entire thorax in *LSL-Kras^{G12D};Trp53$^{fl/fl}$;*CAG-tdTomato mice that received 75 Gy irradiation, with or without 2-ME. At 4 weeks after Ad-Cre administration, horizontal (upper), transaxial (middle), and 3D micro-CT (bottom) images were acquired from nonirradiated animals (0, 4 weeks) and after 75 Gy irradiation (0, 2, 4 weeks). Quantification of normal lung area is shown. (C) Representative images of lungs, immunofluorescence staining of tdTomato (scale bar = 200 μm) and Masson trichrome staining (scale bar = 100 μm), and (D) immunofluorescence staining of αSMA, tdTomato, and CD31 (scale bar = 50 μm, scale bare of cropped images = 10 μm) in lung tissues from (B). Quantification of collagen deposition per field (magnification, 200×) and the αSMA^{+}CD31^{+}/CD31^{+} area as an average of 5 fields (magnification, 100×). Error bars indicate SEM. $^{*}P < .05$, $^{\dagger}P < .01$ (1-way ANOVA for multiple comparison). Data are representative of 3 independent experiments.

In this study, we analyzed the fibrotic phase with collagen composition in the interstitial areas at 2 weeks after 90 Gy-focal irradiation. Previously, it has been reported that extensive collagen with late-stage fibrosis was deposited at 4 weeks after 90 Gy-focal irradiation. In particular, we performed a functional evaluation using a Flexivent system. Inspiratory capacity was decreased significantly at 2 weeks and 4 weeks; decreased hysteresis, and increased tissue damping were prominent at 4 weeks.[11,25] Therefore, we cautiously suggest that 2-ME could have beneficial effects several months after exposure, on the late stage of RIPF.

Radiation-pneumonitis (RP) is considered a common toxicity after SBRT and conventional radiation therapy to the lung,[44] and it can occasionally cause death. In SBRT, planning target volume (PTV) volume and organ motion were correlated with RP.[45] Radiation-induced EndMT is reported to occur in the initial step, before the tissue fibrotic phase during the development of fibrosis.[12] Thus, we cautiously suggest that targeting radiation-induced EndMT may be effective in inhibiting RP. We will examine the effects of 2-ME on RP and conventional RT and SBRT in future studies. Moreover, the model of normal tissue damage caused by ablative high-dose RT in this study is useful for countermeasure development, and 2-ME is suggested to be studied as a countermeasure in high-dose radiation exposure.

A phenotypic change in EndMT causes vascular diseases, such as tissue fibrosis, which promotes cancer-associated fibroblasts in cancer. EndMT may also be accompanied by tumor pericyte coverage[46] and cause tumor resistance to chemotherapy.[47,48] The inhibition of tumor EndMT following RT can suppress lung tumor regrowth and metastases.[19]

As a promising EndMT inhibitor, 2-ME enhanced tumor susceptibility to radiation therapy, with decreased αSMA^{+} $NG2^{+}$ vessel formation. To distinguish the responses of the tumoral region and nontumoral region, we used spontaneous lung tumor models with tracking of tdTomato-expressing tumor cells. This GEMM may be helpful to distinguish the responses of normal cells from a single tumor and multitumor in RIPF development. Additionally, analysis of the radio-response of NSCLCs using FDG-PET suggest that 2-ME inhibits tumor glycolysis in combination with radiation therapy. Targeting HIF-1 and tumor glucose metabolism has been reported to enhance the efficacy of radiation therapy.[49]

Together with the findings of the present study, this suggests that development of strategies to regulate EndMT will provide valuable insights for the enhancement of RT efficacy to reduce RIPF and overcome tumor radio resistance.

Conclusions

It was previously revealed that 2-ME, a HIF-1α inhibitor, efficiently prevents radiation-induced EndMT.[12] As such, both pre- and posttreatment with 2-ME were demonstrated to efficiently inhibit RIPF after ablative focal irradiation, concomitantly reducing EndMT. In the present study, we established a preclinical platform combining GEMM and IGRT to recapitulate human cancer with spontaneous tumors and RT, respectively, for the purpose of evaluating an RIPF inhibitor in radiation therapy for NSCLC. Specifically, a tumor tracing system using tdTomato;K-Ras^{G12D};p53KO mice allowed visualization of easily discernable fibrotic changes between tumoral and normal regions. Our findings highlight the clinical implications of 2-ME in RT for lung cancer, ultimately revealing that 2-ME in combination with RT inhibits the development of RIPF and tumor regrowth in IGRT as shown using single- and multifocal NSCLC mouse models. Notably, these outcomes are likely to be clinically meaningful in both palliative and curative radiation therapies, potentially minimizing normal tissue complications. However, further studies are encouraged to better understand the clinical usefulness of 2-ME in fractioned RT. Nevertheless, the findings presented herein suggest that targeting HIF-1α-mediated EndMT might constitute a viable strategy for lung fibrosis, especially RIPF. In addition, 2-ME, a suggested regulator of HIF-1α-mediated EndMT, may be useful as an effective inhibitor of RIPF in RT.

References

1. Herbst RS, Morgensztern D, Boshoff C. The biology and management of non-small cell lung cancer. *Nature* 2018;553:446-454.
2. Brush J, Lipnick SL, Phillips T, et al. Molecular mechanisms of late normal tissue injury. *Semin Radiat Oncol* 2007;17:121-130.
3. Tyldesley S, Boyd C, Schulze K, et al. Estimating the need for radiotherapy for lung cancer: An evidence-based, epidemiologic approach. *Int J Radiat Oncol Biol Phys* 2001;49:973-985.
4. Rodrigues G, Lock M, D'Souza D, et al. Prediction of radiation pneumonitis by dose-volume histogram parameters in lung cancer—A systematic review. *Radiother Oncol* 2004;71:127-138.
5. Yarnold J, Brotons MC. Pathogenetic mechanisms in radiation fibrosis. *Radiother Oncol* 2010;97:149-161.
6. Thompson M, Rosenzweig KE. The evolving toxicity profile of SBRT for lung cancer. *Transl Lung Cancer Res* 2019;8:48-57.
7. Kang KH, Okoye CC, Patel RB, et al. Complications from stereotactic body radiotherapy for lung cancer. *Cancers (Basel)* 2015;7:981-1004.
8. Mehta V. Radiation pneumonitis and pulmonary fibrosis in non-small-cell lung cancer: Pulmonary function, prediction, and prevention. *Int J Radiat Oncol Biol Phys* 2005;63:5-24.
9. Rube CE, Uthe D, Schmid KW, et al. Dose-dependent induction of transforming growth factor beta (TGF-beta) in the lung tissue of fibrosis-prone mice after thoracic irradiation. *Int J Radiat Oncol Biol Phys* 2000;47:1033-1042.
10. Abdollahi A, Li M, Ping G, et al. Inhibition of platelet-derived growth factor signaling attenuates pulmonary fibrosis. *J Exp Med* 2005;201:925-935.
11. Hong ZY, Lee HJ, Choi WH, et al. A preclinical rodent model of acute radiation-induced lung injury after ablative focal irradiation reflecting clinical stereotactic body radiotherapy. *Radiat Res* 2014;182:83-91.
12. Choi SH, Hong ZY, Nam JK, et al. A hypoxia-induced vascular endothelial-to-mesenchymal transition in development of radiation-induced pulmonary fibrosis. *Clin Cancer Res* 2015;21:3716-3726.
13. Kim JY, An YM, Yoo BR, et al. HSP27 inhibitor attenuates radiation-induced pulmonary inflammation. *Sci Rep* 2018;8:4189.

14. DuPage M, Dooley AL, Jacks T. Conditional mouse lung cancer models using adenoviral or lentiviral delivery of Cre recombinase. *Nat Protoc* 2009;4:1064-1072.
15. Kim M, Choi SH, Jin YB, et al. The effect of oxidized low-density lipoprotein (ox-LDL) on radiation-induced endothelial-to-mesenchymal transition. *Int J Radiat Biol* 2013;89:356-363.
16. Choi SH, Nam JK, Kim BY, et al. HSPB1 inhibits the endothelial-to-mesenchymal transition to suppress pulmonary fibrosis and lung tumorigenesis. *Cancer Res* 2016;76:1019-1030.
17. Hong L, Du X, Li W, et al. EndMT: A promising and controversial field. *Eur J Cell Biol* 2018;97:493-500.
18. van Meeteren LA, ten Dijke P. Regulation of endothelial cell plasticity by TGF-beta. *Cell Tissue Res* 2012;347:177-186.
19. Choi SH, Kim AR, Nam JK, et al. Tumour-vasculature development via endothelial-to-mesenchymal transition after radiotherapy controls $CD44v6^{+}$ cancer cell and macrophage polarization. *Nat Commun* 2018;9:5108.
20. Lakhani NJ, Sarkar MA, Venitz J, et al. 2-Methoxyestradiol, a promising anticancer agent. *Pharmacotherapy* 2003;23:165-172.
21. Tevaarwerk AJ, Holen KD, Alberti DB, et al. Phase I trial of 2-methoxyestradiol NanoCrystal dispersion in advanced solid malignancies. *Clin Cancer Res* 2009;15:1460-1465.
22. Ricker JL, Chen Z, Yang XP, et al. Van Waes, 2-methoxyestradiol inhibits hypoxia-inducible factor 1alpha, tumor growth, and angiogenesis and augments paclitaxel efficacy in head and neck squamous cell carcinoma. *Clin Cancer Res* 2004;10:8665-8673.
23. Mabjeesh NJ, Escuin D, LaVallee TM, et al. 2ME2 inhibits tumor growth and angiogenesis by disrupting microtubules and dysregulating HIF. *Cancer Cell* 2003;3:363-375.
24. Kilkenny C, Browne WJ, Cuthill IC, et al. Improving bioscience research reporting: The ARRIVE guidelines for reporting animal research. *PLoS Biol* 2010;8:e1000412.
25. Hong ZY, Eun SH, Park K, et al. Development of a small animal model to simulate clinical stereotactic body radiotherapy-induced central and peripheral lung injuries. *J Radiat Res* 2014;55:648-657.
26. Kim M, Woo SK, Yu JW, et al. Effect of Harderian adenectomy on the statistical analyses of mouse brain imaging using positron emission tomography. *J Vet Sci* 2014;15:157-161.
27. Ma CM, Coffey CW, DeWerd LA, et al. AAPM protocol for 40-300 kV x-ray beam dosimetry in radiotherapy and radiobiology. *Med Phys* 2001;28:868-893.
28. Ashcroft T, Simpson JM, Timbrell V. Simple method of estimating severity of pulmonary fibrosis on a numerical scale. *J Clin Pathol* 1988;41:467-470.
29. Li C, Li C, Zhang AJ, et al. Avian influenza A H7N9 virus induces severe pneumonia in mice without prior adaptation and responds to a combination of zanamivir and COX-2 inhibitor. *PLoS One* 2014;9:e107966.
30. Helmestam M, Andersson H, Stavreus-Evers A, et al. Tamoxifen modulates cell migration and expression of angiogenesis-related genes in human endometrial endothelial cells. *Am J Pathol* 2012;180:2527-2535.
31. Kouvaris JR, Kouloulias VE, Vlahos LJ. Amifostine: The first selective-target and broad-spectrum radioprotector. *Oncologist* 2007;12:738-747.
32. Margaritopoulos GA, Vasarmidi E, Antoniou KM. Pirfenidone in the treatment of idiopathic pulmonary fibrosis: An evidence-based review of its place in therapy. *Core Evid* 2016;11:11-22.
33. Wenger RH, Stiehl DP, Camenisch G. Integration of oxygen signaling at the consensus HRE. *Sci STKE* 2005;2005:re12.
34. Cowburn AS, Crosby A, Macias D, et al. HIF2α-arginase axis is essential for the development of pulmonary hypertension. *Proc Natl Acad Sci U S A* 2016;113:8801-8806.
35. Gkretsi V, Stylianou A, Papageorgis P, et al. Remodeling components of the tumor microenvironment to enhance cancer therapy. *Front Oncol* 2015;5:214.
36. Linda A, Trovo M, Bradley JD. Radiation injury of the lung after stereotactic body radiation therapy (SBRT) for lung cancer: A timeline and pattern of CT changes. *Eur J Radiol* 2011;79:147-154.
37. Majmundar AJ, Wong WJ, Simon MC. Hypoxia-inducible factors and the response to hypoxic stress. *Mol Cell* 2010;40:294-309.
38. Taniguchi CM, Miao YR, Diep AN, et al. PHD inhibition mitigates and protects against radiation-induced gastrointestinal toxicity via HIF2. *Sci Transl Med* 2014;6:236ra264.
39. Toullec A, Buard V, Rannou E, et al. HIF-1α deletion in the endothelium, but not in the epithelium, protects from radiation-induced enteritis. *Cell Mol Gastroenterol Hepatol* 2018;5:15-30.
40. Wei H, Bedja D, Koitabashi N, et al. Endothelial expression of hypoxia-inducible factor 1 protects the murine heart and aorta from pressure overload by suppression of TGF-beta signaling. *Proc Natl Acad Sci U S A* 2012;109:E841-E850.
41. Bryant AJ, Carrick RP, McConaha ME, et al. Endothelial HIF signaling regulates pulmonary fibrosis-associated pulmonary hypertension. *Am J Physiol Lung Cell Mol Physiol* 2016;310:L249-L262.
42. Huang TQ, Wang Y, Ebrahem Q, et al. Deletion of HIF-1α partially rescues the abnormal hyaloid vascular system in Cited2 conditional knockout mouse eyes. *Mol Vis* 2012;18:1260-1270.
43. Lavigne J, Suissa A, Verger N, et al. Lung stereotactic Arc therapy in mice: Development of radiation pneumopathy and influence of HIF-1α endothelial deletion. *Int J Radiat Oncol Biol Phys* 2019;104:279-290.
44. Yamashita H, Takahashi W, Haga A, et al. Radiation pneumonitis after stereotactic radiation therapy for lung cancer. *World J Radiol* 2014;6:708-715.
45. Ong CL, Palma D, Verbakel WF, et al. Treatment of large stage I-II lung tumors using stereotactic body radiotherapy (SBRT): Planning considerations and early toxicity. *Radiother Oncol* 2010;97:431-436.
46. Medici D, Kalluri R. Endothelial-mesenchymal transition and its contribution to the emergence of stem cell phenotype. *Semin Cancer Biol* 2012;22:379-384.
47. Helfrich I, Scheffrahn I, Bartling S, et al. Resistance to antiangiogenic therapy is directed by vascular phenotype, vessel stabilization, and maturation in malignant melanoma. *J Exp Med* 2010;207:491-503.
48. Franco M, Roswall P, Cortez E, et al. Pericytes promote endothelial cell survival through induction of autocrine VEGF-A signaling and Bcl-w expression. *Blood* 2011;118:2906-2917.
49. Meijer TW, Kaanders JH, Span PN, et al. Targeting hypoxia, HIF-1, and tumor glucose metabolism to improve radiotherapy efficacy. *Clin Cancer Res* 2012;18:5585-5594.